Tracer counterpermeation analysis of diffusivity in finite-length nanopores with and without single-file dynamics

David M. Ackerman[1,2] and James W. Evans[1,3]
[1]*Ames Laboratory—USDOE, Iowa State University, Ames, Iowa 50011, USA*
[2]*Department of Mechanical Engineering, Iowa State University, Ames, Iowa 50011, USA*
[3]*Department of Physics & Astronomy and Department of Mathematics, Iowa State University, Ames, Iowa 50011, USA*
(Received 13 November 2016; published 19 January 2017)

We perform a tracer counterpermeation (TCP) analysis for a stochastic model of diffusive transport through a narrow linear pore where passing of species within the pore is inhibited or even excluded (single-file diffusion). TCP involves differently labeled but otherwise identical particles from two decoupled infinite reservoirs adsorbing into opposite ends of the pore, and desorbing from either end. In addition to transient behavior, we assess steady-state concentration profiles, spatial correlations, particle number fluctuations, and diffusion fluxes through the pore. From the profiles and fluxes, we determine a generalized tracer diffusion coefficient $D_{tr}(x)$, at various positions x within the pore. $D_{tr}(x)$ has a plateau value in the pore center scaling inversely with the pore length, but it is enhanced near the pore openings. The latter feature reflects the effect of fluctuations in adsorption and desorption, and it is also associated with a nontrivial scaling of the concentration profiles near the pore openings.

DOI: 10.1103/PhysRevE.95.012132

I. INTRODUCTION

Starting in the 1950's, interest developed in quantifying transport through finite-length pores traversing biological membranes [1–3]. It was noted that such pores could be sufficiently narrow that passing of diffusing species within the pores could be strongly inhibited. It was subsequently recognized that analogous transport issues apply for separations and catalysis in nanoporous materials, particularly for zeolites [4,5]. The extreme case corresponding to the complete absence of passing in these systems is described as single-file diffusion (SFD). In a fundamental theoretical study of SFD in an infinite system in 1965, Harris [6] rigorously demonstrated the occurrence of anomalous behavior wherein the mean-square displacement of a tagged particle increases like the square root of time. (This contrasts the conventional linear time dependence from Einstein's law.) The anomalous behavior corresponds to a vanishing tracer diffusion coefficient $D_{tr} = 0$ for SFD in an infinite system, and naturally also affects transport in finite SFD systems. Significantly for nanoporous materials, a number of experimental probes are sensitive to SFD dynamics and its impact on concentration profiles, so direct evidence of such anomalous dynamics can be obtained. These probes include pulsed-field-gradient (PFG) nuclear magnetic resonance (NMR) [7–9], hyperpolarized Xe^{129} NMR spectroscopy [10,11] (which can monitor diffusion up to $\sim$10 s versus $\sim$100 ms for PFG NMR, thereby treating systems with lower mobilities), and infrared microimaging and interference microscopy for larger systems with dimensions $\sim 100\ \mu$m [12].

Simulation studies for finite SFD systems with periodic boundary conditions offer the possibility to precisely quantify tracer diffusivity of a tagged particle by tracking the mean-square displacement and applying Einstein's law [13,14]. (Here, displacement must be suitably defined to allow unbounded growth.) Subsequent analyses extended consideration to finite pores with various types of boundary conditions, including free exchange with the environment which is of relevance for the applications described above [15]. In many previous studies, there were no interactions between particles except for steric interactions excluding overlap or passing. Specifically, for discrete lattice-gas-type models, the pore is divided into L adjacent cells each of which can be populated by at most a single particle. Particles can hop left or right to adjacent empty cells with a specified rate h. This prescription of hopping dynamics automatically imposes SFD. For such models, the concentration C corresponds to probability that a cell is occupied, so that $0 \leqslant C \leqslant 1$. Then, various studies (above) revealed that the *overall tracer diffusivity* for the pore of L cells has the form [14,15]

$$D_{tr} \approx D_0(1-C)/(CL), \quad \text{for large } L. \tag{1}$$

Here, $D_0 = a^2 h$ denotes the diffusivity in the zero-coverage limit, where "a" denotes the cell width (or lattice spacing) which is set to unity below. Thus, the effect of SFD is reflected in the C dependence as well as the inverse proportionality to pore length L. Refinements to (1) have been suggested for smaller L [14–16], a particularly effective version of which appears to be that in Ref. [17].

A significant development in the analysis of inhibited diffusion for finite systems with free exchange with the environment was the consideration and analysis by Nelson and Auerbach of a so-called tracer counterpermeation (TCP) process [18]. In general terms, TCP applies to porous systems of finite width connected on either side to infinite well-stirred reservoirs which are decoupled from each other. The system involves a single type of diffusing particle (in terms of interactions and diffusional dynamics), but particles in different reservoirs are labeled so as to be distinguishable. Particles in the left (right) reservoir diffuse through the finite porous system into the right (left) reservoir where they are immediately infinitely diluted (and thus do not reenter the porous system). The system reaches a steady state with concentration profiles for the labeled particles varying roughly linearly with position x across the porous system. Measurement of the flux of labeled particles through the porous system together with the local concentration gradient yields a local or *generalized tracer diffusivity* $D_{tr}(x)$. This $D_{tr}(x)$ is approximated by (1) in the

system interior, but it is enhanced near the edges, especially for SFD. These features are of central interest in the current study.

As an aside, we also note that recently a different strategy was introduced to analyze generalized tracer diffusivity in these above types of systems based on tracking of a tagged walker [19,20]. The tagged walker starts at a specified location x inside the porous system of finite width and wanders among a prescribed density of untagged particles. It is also specified to remain at the boundary once exiting the porous system. One tracks the root-mean-square (RMS) displacement and determines an "exit time" T_x, based on when the RMS displacement increases to the distance of the closest boundary. Then, taking $D_{\rm tr}(x) \propto (T_x)^{-1}$, one finds that $D_{\rm tr}(x)$ exhibits the same features as determined from a TCP analysis. This tagged walker approach has some advantages in applying directly to semi-infinite systems, and also in elucidating the form of $D_{\rm tr}(x)$.

Finally, we also mention that it is well recognized that there are different temporal regimes of tracer diffusivity in finite SFD systems with conventional diffusion occurring for short times crossing over to SFD for moderate times, and potentially to center-of-mass diffusion for long times [11,15,17,21]. The latter crossover depends on location of the tagged particle within the pore, behavior reminiscent of the above position dependence on tracer diffusivity.

Now, we return to the *general analysis of TCP processes*, which is the central focus of this paper. It should be emphasized that TCP steady states are not fully described by concentration profiles and fluxes alone, although these do suffice to determine $D_{\rm tr}(x)$. For a more complete characterization, spatial correlations and associated particle number fluctuations should also be assessed, although it appears that this has not been done previously. Spatial correlations have, however, been characterized in somewhat related nonequilibrium systems. Some of these involve single-component noninteracting lattice gases for finite or semi-infinite noninteracting systems coupled to reservoirs having a different particle density [22–24]. Here, negative anticlustering correlations develop under relaxation, although these features do not reflect tagged-particle or SFD dynamics. Perhaps closer to the TCP scenario are finite or semi-infinite lattice-gas reaction-diffusion systems with SFD or less restrictive inhibited passing. In these systems, reaction induces subtle positive clustering correlations [19,25].

In this contribution, we analyze TCP for a one-dimensional noninteracting lattice-gas model for inhibited transport within a pore, which includes SFD as a special case. We consider both steady-state behavior, and also evolution starting from a natural uncorrelated initial state with exactly linear concentration profiles. In particular, we extract the tagged-particle steady-state concentration profiles and flux through the pore allowing assessment of the generalized tracer diffusivity $D_{\rm tr}(x)$. We demonstrate convergence to a well-defined limiting behavior of concentration profiles near pore openings as the pore length increases. We also compare TCP results for $D_{\rm tr}(x)$ with those from the tagged walker approach. Beyond these basic studies of TCP profiles, we assess particle number fluctuations, spatial correlations, and other characterizations of steady-state configurations. In Sec. II, we describe our stochastic model and our choice of initial state for TCP analysis, and illustrate

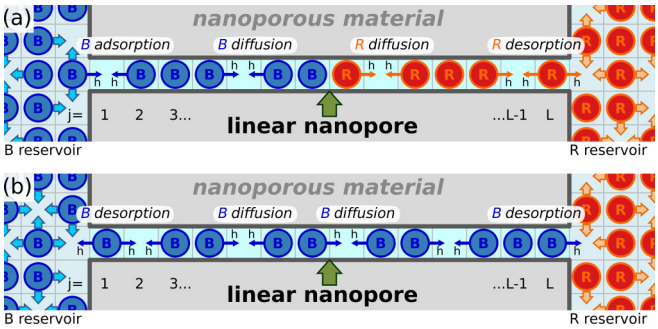

FIG. 1. Schematic of TCP steady-state configurations for SFD: (a) configuration with interface between B-filled and R-filled regions of the pore in the middle of the pore; (b) configuration with the pore only populated by B allowing B desorption into the R reservior.

basic results for steady-state profiles. In Sec. III, we briefly provide some theoretical background for our TCP analysis presenting fundamental evolution equations, and discussing spatial correlations, particle number fluctuations, and the formulation of generalized tracer diffusivity. Results for model behavior from kinetic Monte Carlo (KMC) simulations are presented in Sec. IV. Conclusions are presented in Sec. V.

II. TRACER COUNTERPERMEATION (TCP) MODEL

Our stochastic model is illustrated schematically in Fig. 1. A narrow linear pore is divided into L adjacent cells. The pore is connected at each end to infinite reservoirs which can be represented by three-dimensional arrays of cells. All cells are populated by at most a single particle. Within the pore, particles can hop to nearest-neighbor (NN) empty cells at rate h (per direction). In general, pairs of particles on NN cells can also exchange places at rate $P_{ex}h$. Thus, $P_{ex} = 0$ corresponds to SFD, and $P_{ex} = 1$ corresponds to uninhibited passing. Both hopping and exchange processes with the above rates also apply for pairs of sites where one is just inside the pore and the other is just outside.

Infinite reservoirs adjacent to the left and right ends of the pore are decoupled from each other, and particles in these reservoirs are labeled or colored differently, blue (B) and red (R), respectively. The reservoirs are regarded as being well stirred, and thus to have a random distribution of particles at a fixed concentration $\langle X_0 \rangle$. (One can regard this equilibration as being the result of very rapid hopping of particles within the reservoirs to adjacent empty cells.) As a result, B-type (R-type) particles reaching the right (left) reservoir are immediately infinitely diluted and do not reenter the pore. Also, given this reservoir dynamics, it follows that the rate for a particle at end cells within the pore to exit or desorb from the pore is given by $w_{\rm des} = h(1 - \langle X_0 \rangle)$. The rate at which a reservoir particle just outside the pore enters or adsorbs at an empty end site within the pore is given by $w_{\rm ads} = h\langle X_0 \rangle$. Thus, it is clear that it suffices to just simulate the state within the pore (not the reservoirs) with the appropriate adsorption and desorption rates.

In this study, we consider a *specific initial value problem* starting with exactly linear concentration profiles of blue (red) particles decreasing from $\langle X_0 \rangle$ just outside one end of the pore to zero just outside the other from left to right (from right

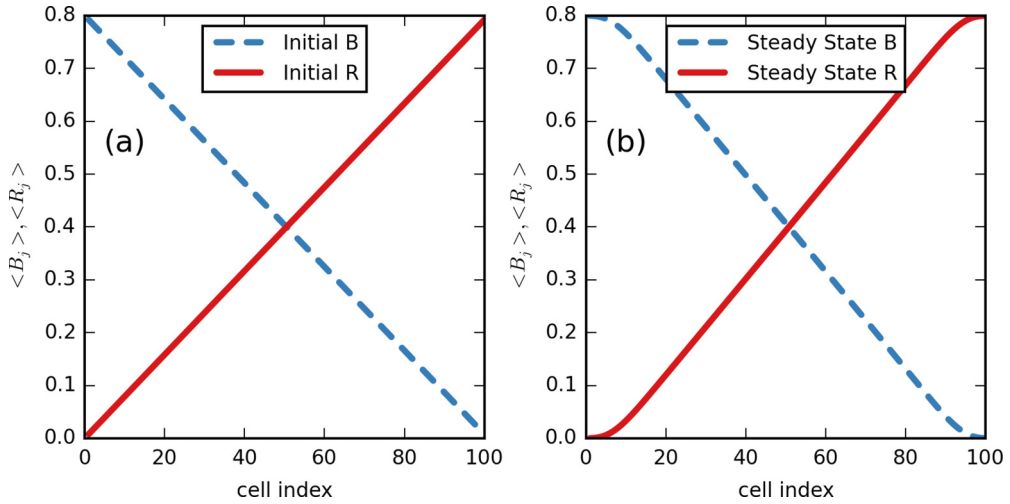

FIG. 2. Concentration profiles for B and R particles for SFD with $L = 100$ and $\langle X_0 \rangle = 0.8$: (a) the initial uncorrelated state with linear profiles; and (b) the final correlated steady state for TCP.

to left) along the pore. In addition, pore sites are populated randomly with the appropriate concentrations, so there are *no spatial correlations* in the initial state. Consequently, initially particles are not strictly ordered with red on the right and blue on the left within the pore, although it is more likely to find red (blue) on the right (left). The system then evolves to reach the true TCP steady state where concentration profiles are roughly but not exactly linear, and where particles are strictly ordered. See Fig. 2. Precise analysis of evolution in this system is achieved with the aid of KMC simulations. Some details of the KMC algorithm are provided in Appendix A. Certainly, other initial conditions could be chosen [26], which of course will not impact final steady-state behavior. However, the above choice is particularly natural in terms of ensuring simple evolution to the steady state, as discussed further below.

Next, we comment on a "color-blind" analysis of behavior where one cannot distinguish between differently colored or labeled particles. For the corresponding single-component system, it is clear that the initial uncorrelated state with uniform concentration (both inside the pore and in the reservoirs) also corresponds to the final steady state. Thus, for our specific choice of initial conditions, there is no evolution of the total concentration from its initial uniform state, and there is no development of nonzero color-blind spatial correlations for particles X (i.e., correlations retain their zero initial values). The same would apply to other random initial conditions provided that they also start with a uniform total concentration [26]. However, for other choices such as starting with an empty pore, there will be natural evolution governed by the simple diffusion equation of the concentration profile to a uniform state (see Sec. III A). There would generally be a subtle and transient development of negative anticlustering spatial correlations [22–24], where these ultimately vanish in the steady state.

Finally, we emphasize that while color-blind spatial correlations for particles X do not develop for our selected initial conditions, this is not the case for correlations associated with labeled or colored particles, B and R. In Sec. IV, we show that spatial correlations do develop for the latter.

III. THEORY: CONCENTRATIONS, FLUCTUATIONS, CORRELATIONS, AND DIFFUSIVITY

A. Master equations for concentrations and related quantities

Within the linear pore, we label cells from left to right by $j = 1$ to L. Let $B_j(R_j) = 1$ correspond to a blue (red) particle in cell j, where $B_j(R_j) = 0$ otherwise. Thus, $X_j = B_j + R_j = 1(0)$ if cell j is occupied (empty), and $E_j = 1 - X_j = 0\,(1)$ if cell j is empty (occupied). Below, we let $C = B$, R, or X. Then, $N_C = \sum_{1 \leqslant j \leqslant L} C_j$ gives the total number of C-type particles in the pore. If $\langle\rangle$ denotes an appropriate ensemble average, then $\langle C_j \rangle$ denotes the probability that cell j is occupied by a type C particle (i.e., the local concentration of such particles). Also, it follows that $\langle X_j \rangle = \langle B_j \rangle + \langle R_j \rangle$, and $\langle X_j \rangle + \langle E_j \rangle = 1$. We also adopt a natural notation for the probabilities of multicell configurations, e.g., $\langle B_j E_{j+1} \rangle$ denotes the probability that cell j is occupied by B and cell $j + 1$ is empty. The evolution of $\langle B_j \rangle$, $\langle R_j \rangle$, and more complicated multicell probabilities is described by an exact set of hierarchical master equations. For example, for $1 < j < L$, one has that

$$d/dt \langle B_j \rangle = -\nabla J_B(j > j+1), \tag{2}$$

where

$$J_B(j > j+1) = h[\langle B_j E_{j+1} \rangle - \langle E_j B_{j+1} \rangle] + P_{ex} h[\langle B_j R_{j+1} \rangle - \langle R_j B_{j+1} \rangle], \tag{3}$$

and $\nabla K_j = K_j - K_{j-1}$ is a discrete derivative. Here $J_B(j > j+1)$ denotes the net flux of B from cell j to cell $j+1$. There are analogous equations for $\langle R_j \rangle$ with $1 < j < L$. Both sets of equations are supplemented by modified equations for the end sites $j = 1$ and $j = L$ appropriately accounting for adsorption and desorption processes. Separate equations can be obtained for the two-cell pair probabilities appearing in the flux terms which couple to triple-cell probabilities, etc. Two-cell spatial correlations control the flux, and we find that these are significant for small P_{ex} [19,20].

Despite the last observation, it is instructive to consider mean-field (MF) type factorization approximations to the

above equations. In the simplest site approximation, one ignores all spatial correlations, so that $\langle B_j E_{j+1}\rangle \approx \langle B_j\rangle\langle E_{j+1}\rangle$, etc. Then, after utilizing this factorization, noting that $\langle E_j\rangle = 1 - \langle X_0\rangle$, and also incorporating some simplifying cancellation, one obtains

$$J_B(j > j+1)|_{\text{site}} = -h[(1-\langle X_0\rangle) + P_{ex}\langle X_0\rangle]\nabla\langle B_j\rangle. \quad (4)$$

Together with the theoretical formulation to be presented in Sec. III C, this result implies a position-independent tracer diffusivity,

$$D_{\text{tr}}(\text{site}) = D_0[(1-\langle X_0\rangle) + P_{ex}\langle X_0\rangle]. \quad (5)$$

We will argue below that $D_{\text{tr}}(\text{site})$ might be expected to provide an upper bound to the actual position-dependent generalized tracer diffusivity. We should note that this mean-field treatment becomes exact when $P_{ex} = 1$ so passing is completely unhindered and $D_{\text{tr}} = D_0$.

Finally, we also note that adding equations for $\langle B_j\rangle$ and $\langle R_j\rangle$ yields classic discrete diffusion equations for $d/dt\langle X_j\rangle = -\nabla J_X(j > j+1)$ where $J_X(j > j+1) = -h\nabla\langle X_j\rangle$ exploiting an exact cancellation of pair probability terms [19,27]. For the initial value problem considered in this study, at $t = 0$ for all j, we set $\langle X_j\rangle = \langle X_0\rangle$ the external reservoir concentration, and thus these quantities do not change in time.

B. Particle number fluctuations and spatial correlations

In this study, we have a particular interest in characterizing particle number fluctuations and the associated spatial correlations. For $C = B$, R, or X, using that $\langle (C_j)^2\rangle = \langle C_j\rangle$, one obtains the general fluctuation-correlation relation

$$\begin{aligned}\text{Var}(N_C) &= \langle (N_C - \langle N_C\rangle)^2\rangle \\ &= \Sigma_i\langle C_i\rangle(1-\langle C_i\rangle) + \Sigma\Sigma_{i\neq j}\text{Cov}(C_i, C_j), \quad (6)\end{aligned}$$

where the covariance $\text{Cov}(C_i,C_j) = \langle C_iC_j\rangle - \langle C_i\rangle\langle C_j\rangle$ corresponds to a two-point spatial correlation function for C-type particles. The sums in (6) range over all cells in the pore. There are a few basic results that follow from this relation, and which are particularly relevant for our study, as described below.

First, we consider "color-blind" fluctuations in the total number of particles X for any initial conditions with uniform total concentration and uncorrelated initial particle distributions [26]. This includes our choice with linear concentration profiles for B and R in Sec. II, but can also cover nonlinear profiles. We have already indicated in Sec. II that $\text{Cov}(X_i,X_j) = 0$ for $i \neq j$ not just for $t = 0$, but for all $t \geqslant 0$; i.e., no correlations develop. Then, since also $\langle X_j\rangle = \langle X_0\rangle$ for all $t \geqslant 0$, one finds from (6) that

$$\text{Var}(N_X) = L\langle X_0\rangle(1-\langle X_0\rangle) \text{ is constant}, \quad \text{for all } t \geqslant 0. \quad (7)$$

This appealing and simplifying feature is specific to this class of initial conditions.

Second, for any random choice of initial state [26], not only are there no spatial correlations for X-type particles, but also no correlations for B- or R-type particles. Thus, one has that $\text{Cov}(C_i,C_j) = 0$ for $i \neq j$, so that $\text{Var}(N_C) = \sum_i\langle C_i\rangle(1-\langle C_i\rangle)$ for $C = B$ or R can be determined given the initial concentration profiles [26]. For example, one can readily exactly evaluate this sum for our prescribed initial linear profiles in Sec. II. Actually for our purposes assuming that L is not too small, it suffices to approximate this sum by an integral to obtain

$$\text{Var}(N_B) = \text{Var}(N_R) \approx \tfrac{1}{2}L\langle X_0\rangle[1\text{–}(2/3)\langle X_0\rangle], \quad \text{at } t = 0 \text{ for linear profiles}. \quad (8)$$

Unlike $\text{Var}(N_X)$, we will see that $\text{Var}(N_B) = \text{Var}(N_R)$ varies strongly with time t, but the above analysis at least clarifies the initial value.

Third, another basic result for particle number fluctuations which follows simply from the relation $N_X = N_B + N_R$ for any choice of initial condition is that

$$\text{Var}(N_X) = \text{Var}(N_B) + \text{Var}(N_R) + 2\text{Cov}(N_B,N_R), \quad \text{for all } t \geqslant 0, \quad (9)$$

where $\text{Cov}(N_B,N_R) = \langle N_BN_R\rangle - \langle N_B\rangle\langle N_R\rangle$. Consider any choice of random initial conditions with reflection symmetry of B and R concentration profiles about the pore center, including our choice in Sec. II of linear profiles. Then it follows that $\langle B_j\rangle = \langle R_{L-j+1}\rangle$ for all $t \geqslant 0$, so that $\langle N_B\rangle = \langle N_R\rangle$ and $\text{Var}(N_B) = \text{Var}(N_R)$ for all $t \geqslant 0$. Incorporating the latter identity into (9), one obtains

$$\text{Var}(N_X) = 2[\text{Var}(N_B) + \text{Cov}(N_B,N_R)], \quad \text{for all } t \geqslant 0. \quad (10)$$

We find that clustering correlations develop for B and R particles, i.e., $\text{Cov}(C_i,C_j) > 0$ for $C = B$ or R, and in fact positive $\text{Var}(N_B) = \text{Var}(N_R)$ is large relative to positive $\text{Var}(N_X)$. On the other hand, anticlustering correlations develop between B and R particles, i.e., $\text{Cov}(B_i,R_j) < 0$, so that $\text{Cov}(N_B,N_R) < 0$. It also follows from (9) that $\text{Cov}(N_B,N_R)$, like $\text{Var}(N_B)$, necessarily has a magnitude much larger than $\text{Var}(N_X)$. Also, significantly, since $\text{Var}(N_X)$ is constant in time, the variation in time of $\text{Cov}(N_B,N_R)$ is determined by that of $\text{Var}(N_B) = \text{Var}(N_R)$ (or vice versa).

C. From hydrodynamic transport theory to generalized tracer diffusivity

Here, we will exploit a fundamental result for transport in diffusive noninteracting lattice-gas systems with particles labeled by two colors, B and R, but otherwise having identical interactions and diffusive dynamics. In the so-called hydrodynamic regime of low-concentration gradients, one regards local concentrations $\langle B\rangle$, $\langle R\rangle$, and $\langle X\rangle = \langle B\rangle + \langle R\rangle$ as functions of a continuous spatial variable x. One would identify $x = ja$ for cell index j in one dimension (1D) where "a" is the cell spacing. Then a rigorous treatment of collective diffusion yields for the diffusion flux of B particles [28,29],

$$\begin{aligned}J_B = &-D_0[(\langle B\rangle/\langle X\rangle)\nabla\langle X\rangle] - D_{\text{tr}}[(\langle R\rangle/\langle X\rangle)\nabla\langle B\rangle \\ &-(\langle B\rangle/\langle X\rangle)\nabla\langle R\rangle], \quad (11)\end{aligned}$$

where ∇ is the gradient operator (so $\nabla = \partial/\partial x$ in 1D), and $\langle X\rangle = \langle B\rangle + \langle R\rangle$ is the total concentration. Here D_0 (D_{tr}) is the collective (tracer) diffusion coefficient for the corresponding single-component system. An analogous expression applies for J_R.

For the case of interest here with hopping to NN empty cells at rate h, and exchange at rate $P_{\text{ex}}h$, one has that $D_0 = a^2h$ is independent of both concentration and P_{ex}.

However, D_{tr} exhibits a nontrivial decrease with decreasing P_{ex} and with increasing concentration. See Ref. [30] for further characterization of D_{tr}. An immediate consequence of (11) for TCP with position-independent $\langle X\rangle$ is that

$$J_B = -D_{tr}\nabla\langle B\rangle \quad \text{and} \quad J_R = -D_{tr}\nabla\langle R\rangle; \tag{12}$$

i.e., in this case, collective diffusion is controlled entirely by tracer diffusivity. See Refs. [17,18] for an alternative derivation of these results.

It is natural to translate and generalize these latter relations for fluxes to a discrete lattice setting for TCP by defining a position-dependent generalized tracer diffusion coefficient for each NN pair $(j, j+1)$ of cells as [18,19]

$$D_{tr}(j, j+1) = -J_B/\nabla\langle B_j\rangle = -J_R/\nabla\langle R_j\rangle. \tag{13}$$

Clearly, this $D_{tr}(j, j+1)$ is symmetric about the pore center. We emphasize here that $J_B = -J_R$ is constant throughout the pore in the TCP steady state. Furthermore, these constant fluxes equal the exit flux of species from the pore, i.e.,

$$J_R = -w_{des}\langle R_1\rangle \quad \text{and} \quad J_B = w_{des}\langle B_L\rangle, \tag{14}$$

so that the fluxes are completely determined by end-cell concentrations. Inspection of Fig. 2(b) immediately reveals that $D_{tr}(j, j+1)$ will adopt a constant minimum plateau value, $D_{tr}(\text{min})$, in the pore center where the concentration profiles for TCP are linear. However, $D_{tr}(j, j+1)$ will be enhanced near the pore openings where concentration gradients are reduced in amplitude.

For SFD ($P_{ex} = 0$), it is reasonable to expect that at least for large L, $D_{tr}(\text{min})$ should correspond to the value predicted for the overall pore tracer diffusivity in (1) with $C = \langle X_0\rangle$. Then, approximating the concentration gradient near the pore center by $\nabla\langle R_{j\approx L/2}\rangle \approx \langle X_0\rangle/L$, one concludes that for SFD, the TCP end-cell concentrations satisfy

$$\langle R_1\rangle = \langle B_L\rangle \approx 1/L^2, \quad \text{for large } L \text{ (for SFD)}. \tag{15}$$

According to the above analysis, these concentrations should be roughly independent of $\langle X_0\rangle$. In fact, our simulation results in Sec. IV C will reveal the scaling behavior $\langle R_j\rangle \approx r(j)/L^2$ for large L, where $r(j)$ is independent of L and increases faster than linearly with j.

Refinements of the result (15) are appropriate to account for finite-length corrections and for low reservoir concentrations. More specifically, these become significant for $\langle X_0\rangle L = O(1)$ where on average there is on the order of one particle (or less) in the pore. These refined results can be obtained from modified versions of (1) such as that given in Ref. [10], and from alternative concentration gradient estimates [31]. They imply a crossover from (15) to $\langle R_1\rangle \approx \langle X_0\rangle/L$ for $\langle X_0\rangle L \ll 1$ ensuring that $D_{tr} \approx D_0$ in this low-concentration regime.

IV. KMC SIMULATION RESULTS

In the following, we focus on behavior for SFD ($P_{ex} = 0$). First, we discuss particle number fluctuations in Sec. IV A and associated spatial correlations in Sec. IV B. These quantities are of fundamental interest in characterizing nonequilibrium steady states. Furthermore, assessment of their transient behavior provides a valuable tool for assessing the onset of the steady state (which is needed in precise analysis of steady-state properties avoiding corruption by transients) as exploited in Sec. IV C. Finally, in Sec. IV D, we present limited results allowing passing of particles within the pore ($P_{ex} > 0$). Again, details of the KMC simulation algorithm are described in Appendix A.

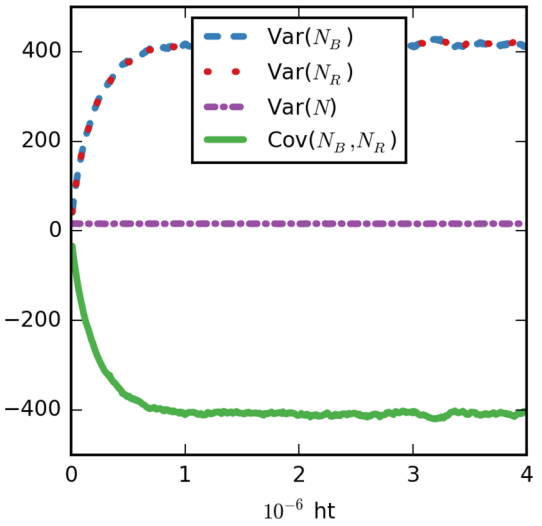

FIG. 3. SFD results for time evolution of particle number fluctuations for $\langle X_0\rangle = 0.8$ and $L = 100$. Behavior is shown for ht from 0 to 4×10^6.

A. Particle number fluctuations for SFD

For SFD with $\langle X_0\rangle = 0.8$ and $L = 100$, the evolution of particle number fluctuations from their values for the uncorrelated initial state towards steady-state values is shown in Fig. 3. Exact initial values for the quantities shown are given by (7) and (8). A key feature is the development of large amplitude fluctuations in N_B and N_R relative to those for N, i.e., $\text{Var}(N_B) = \text{Var}(N_R) \gg \text{Var}(N)$, which reflects clustering rather than a random distribution of species B and R. The correspondingly large negative steady-state value of $\text{Cov}(N_B, N_R)$ is determined by the identity (9).

Elucidation and rough estimation of steady-state values of $\text{Var}(N_B)$ or $\text{Var}(N_R)$ come from recognition of the feature for SFD that all configurations within the pore have B particles to the left and R particles to the right with an interface between B and R particles somewhere within the pore. Given the quasilinear concentration profiles for B and R particles, it follows that the location $x = j$ (setting $a = 1$) of this interface within the pore is described by a uniform (constant) normalized probability distribution, $p(x) = 1/L$ in a natural lowest-order approximation. For location x, the mean total number of B and R particles in the pore is roughly $\langle N_B(x)\rangle \approx (L-x)\langle X_0\rangle$ and $\langle N_R(x)\rangle \approx x\langle X_0\rangle$, respectively. Thus, provided that L is not too small, one estimates for $C = B$ or R that

$$\langle (N_C)^m\rangle \approx \int_{0<x<L} dx p(x)\langle N_C(x)\rangle^m, \quad \text{and}$$
$$\langle N_B N_R\rangle = \int_{0<x<L} dx p(x)\langle N_B(x)\rangle\langle N_R(x)\rangle. \tag{16}$$

From these relations, one can evaluate steady-state $\mathrm{Var}(N_C) = \langle (N_C)^2 \rangle - \langle N_C \rangle^2$ and $\mathrm{Cov}(N_B, N_R)$ to obtain

$$\mathrm{Var}(N_B) = \mathrm{Var}(N_R) \approx \langle X_0 \rangle^2 L^2/12, \text{ and}$$
$$\mathrm{Cov}(N_B, N_R) \approx -\langle X_0 \rangle^2 L^2/12. \quad (17)$$

This analysis predicts that $\mathrm{Var}(N_B) = \mathrm{Var}(N_R) = -\mathrm{Cov}(N_B, N_R) \approx 530$ for SFD with $\langle X_0 \rangle = 0.8$ and $L = 100$ compared with the simulated value of around 420. This indicates that our approximate formulation captures at least the key features of behavior. Both of these values far exceed the much smaller exact value of $\mathrm{Var}(N) = 16$, where we also note that (17) does not exactly reproduce the relation (9).

We emphasize that the above characterization of ordered steady-state configurations (with B to the left and R to the right) does not apply for our choice in Sec. II of random initial state with linear concentration profiles of B and R. In that case, such ordering is not imposed. Consequently, the much smaller initial $\mathrm{Var}(N_B) = \mathrm{Var}(N_R) \approx 18.7$ are given by (8) rather than (17).

Another issue related to our analysis of particle number correlations is a determination of the characteristic time scale t_c for reaching the steady state, recalling that $\mathrm{Var}(N_B) = \mathrm{Var}(N_R)$ and $\mathrm{Cov}(N_B, N_R)$ necessarily relax at the same rate. It has been suggested previously that t_c corresponds to the intracrystalline residence time L^2/D_{tr} which, using (1), implies that $t_c \sim L^3$ [17]. Results presented below appear consistent with this scaling behavior. Reliable assessment of this transient regime is important to enable precise determination of steady-state flux and concentration gradients which in turn determine $D_{\mathrm{tr}}(x)$.

B. Spatial correlations for SFD

We have considered in detail NN pair correlations, $\mathrm{Cov}(B_j, B_{j+1}) = \langle B_j B_{j+1} \rangle - \langle B_j \rangle \langle B_{j+1} \rangle$. For SFD with $\langle X_0 \rangle = 0.8$ and $L = 100$, Fig. 4 shows the development of these correlations (from their zero initial values) on the same time scale, t_c, as the achievement of steady-state behavior for particle number fluctuations. Elucidation and rough estimation of this behavior comes from adopting the above characterization of the ensemble of steady-state configurations with B on the left and R on the right separated by an interface at position x with uniform probability distribution $p(x)$. Again setting $a = 1$, it follows that

$$\langle B_j \rangle \approx \int_{j<x<L} p(x) \langle X_0 \rangle = (1 - j/L) \langle X_0 \rangle, \quad (18)$$

and

$$\langle B_j B_{j+1} \rangle \approx \int_{j<x<L} p(x) \langle X_0 \rangle^2 = (1 - j/L) \langle X_0 \rangle^2, \quad (19)$$

since the interface must be to the right of site j for the configuration to contribute to these quantities. With an analogous analysis for $\mathrm{Cov}(R_j, R_{j+1})$, we conclude that in the steady state one has

$$\mathrm{Cov}(B_j, B_{j+1}) = \mathrm{Cov}(R_j, R_{j+1}) \approx (j/L)(1 - j/L) \langle X_0 \rangle^2. \quad (20)$$

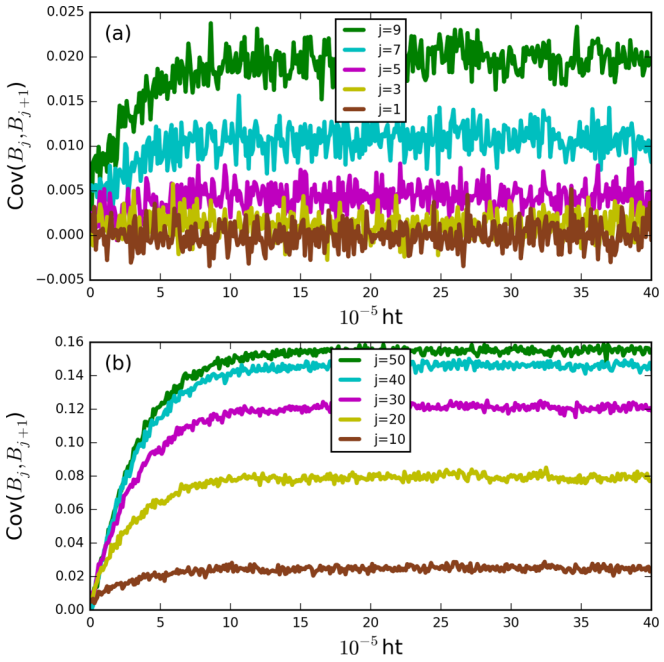

FIG. 4. Evolution of NN pair correlations for SFD with $\langle X_0 \rangle = 0.8$ and $L = 100$: (a) $\mathrm{Cov}(B_j, B_{j+1})$ for cells $j = 1$ to 9 at the end of the pore (from bottom to top); (b) $\mathrm{Cov}(B_j, B_{j+1})$ for cells $j = 10, 20, \ldots,$ and 50 (from bottom to top). Behavior is shown for ht from 0 to 4×10^6.

This analysis predicts that the maximum value $\langle X_0 \rangle^2/4 = 0.16$ for $\langle X_0 \rangle = 0.8$ occurs for $j = L/2$. This prediction is quite close to the KMC estimate of 0.155.

In fact, the above analysis can be readily extended to assess more general two-point spatial correlations in the steady state to obtain

$$\mathrm{Cov}(B_j, B_{j+k}) = \mathrm{Cov}(R_j, R_{j+k}) \approx (j/L)(1 - j/L - k/L) \langle X_0 \rangle^2 > 0, \quad (21)$$

$$\mathrm{Cov}(B_j, R_{j+k}) \approx -(1 - j/L)(j/L + k/L) \langle X_0 \rangle^2 < 0, \quad (22)$$

and

$$\mathrm{Cov}(R_j, B_{j+k}) \approx -(j/L)(1 - j/L - k/L) \langle X_0 \rangle^2. \quad (23)$$

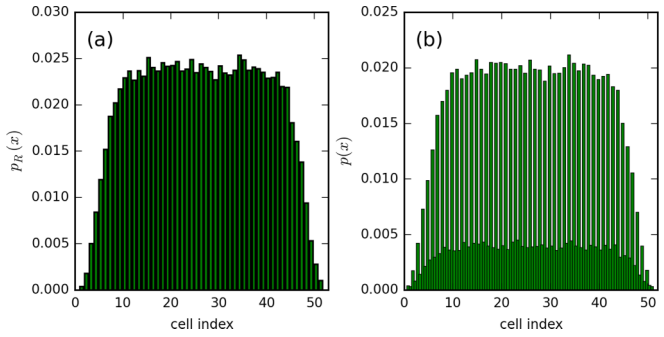

FIG. 5. Interface location distribution for SFD with $\langle X_0 \rangle = 0.8$ and $L = 50$.

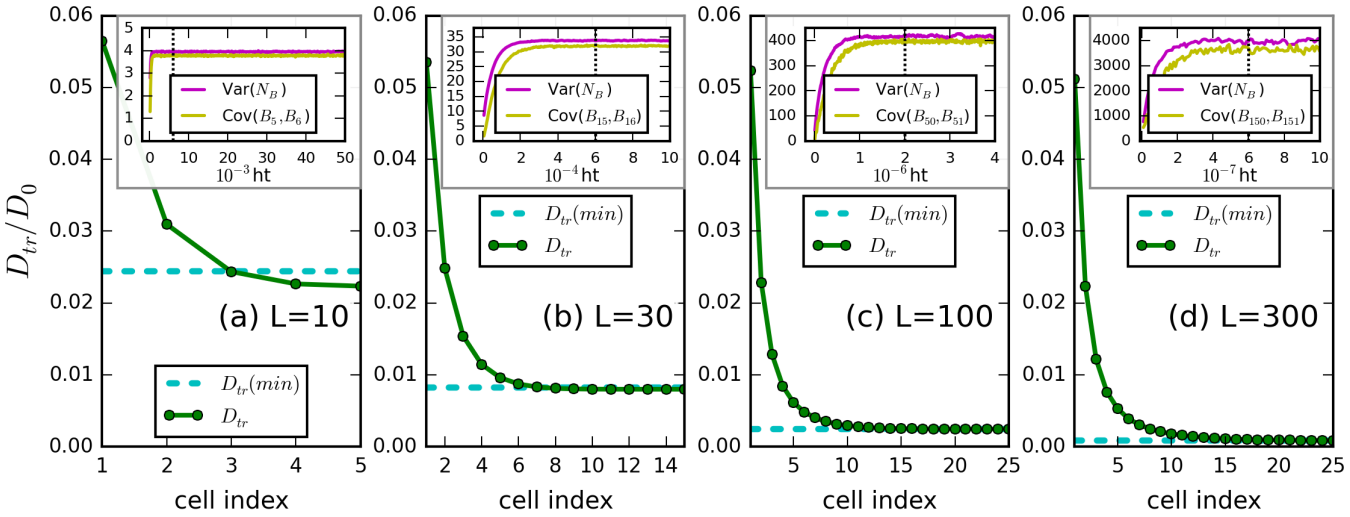

FIG. 6. $D_{tr}(j,j+1)/D_0$ versus cell index j at the left end of the pore for SFD with $\langle X_0\rangle = 0.8$. Dashed horizontal blue line: estimate $D_0(1-\langle X_0\rangle)/[1+\langle X_0\rangle(L-1)]$ of D_{tr}(min). Insets: Var(N_B) and rescaled Cov($B_{L/2},B_{L/2+1}$) [by 34.62, 222.56, 2559.6, and 24066 for $L = 10$, 30, 100, and 300, respectively]. Behavior is shown for ht from 0 to 5×10^4, 10^5, 4×10^6, and 10^8 for $L = 10$, 30, 100, and 300, respectively. The dashed vertical black line shows the onset of the steady state.

The last result is trivial since $\langle R_j B_{j+k}\rangle = 0$ in the steady state. The positive (negative) covariance for pairs of particles of the same (different) types is consistent with and supports the statements made in Sec. IV A.

C. Characterization of steady-state pore configurations for SFD

We have noted above that steady-state configurations within the pore are ordered in that B particles are on the left and R are on the right. We also introduce the location, x, of the interface between B and R populated regions within the pore which in a simple low-order coarse-grained picture is described by a uniform probability distribution, $p(x) = 1/L$. One might expect that $p(x)$ is not exactly uniform due to "edge effects" at the pore openings. Thus, here we provide a more precise analysis.

First, we must precisely define the interface between B and R regions. Perhaps the simplest choice is to define the location as the leftmost R particle (or the rightmost B particle) which just adopts integer values. If there are no R (B) particles in the pore, then we define the interface location as $j = L+1 (j = 0)$. Results are shown in Fig. 5(a) for this distribution, $p_R(x)$, for R particles for $\langle X_0\rangle = 0.8$ and $L = 50$. These do indicate a uniform distribution except near pore openings.

A more appealing symmetric definition takes the position of the interface to be midway between the rightmost B particle and the leftmost R particle in the case where the pore is populated by both B and R particles. Note that this position can adopt both integer and half-integer values. We use the same definition if the pore has no R (B) particles, but assign the position of the rightmost R (leftmost B) particle

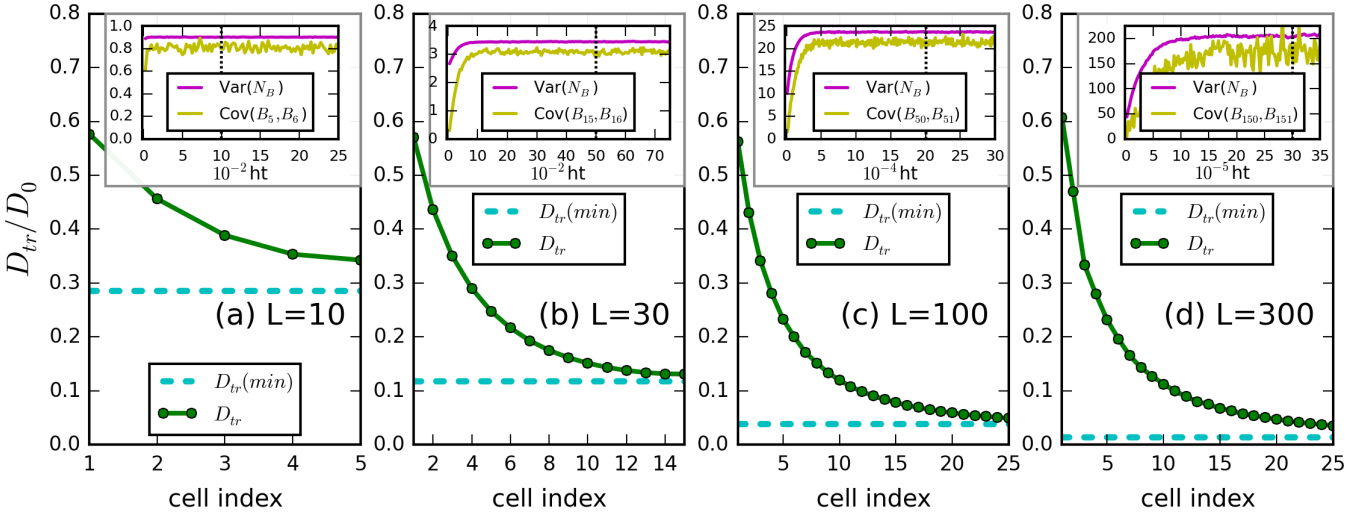

FIG. 7. $D_{tr}(j,j+1)/D_0$ versus cell index j at the left end of the pore for SFD with $\langle X_0\rangle = 0.2$. Dashed horizontal blue line: estimate $D_0(1-\langle X_0\rangle)/[1+\langle X_0\rangle(L-1)]$ of D_{tr}(min). Insets show Var(N_b) and a rescaled Cov($B_{L/2},B_{L/2+1}$) [by 34.62, 222.56, 2559.6, and 24 066 for $L = 10$, 30, 100, and 300, respectively]. Behavior is shown for ht from 0 to 2.5×10^3, 7×10^3, 3×10^5, and 3.5×10^6 for $L = 10$, 30, 100, and 300, respectively. The dashed vertical black line shows the onset of the steady state.

TABLE I. Selected KMC results for SFD with various L. KMC $\langle R_1\rangle$ with analytic estimate in parentheses. KMC flux from counting particles traveling through the pore. KMC $D_{\rm tr}$(min) with analytic estimate in parentheses. Behavior is shown for $\langle X_0\rangle = 0.8, 0.2$.

$\langle X_0\rangle = 0.8$	$\langle R_1\rangle$	J_B	$D_{\rm tr}$(min)	$\langle X_0\rangle = 0.2$	$\langle R_1\rangle$	J_B	$D_{\rm tr}$(min)
$L = 10$	1.23×10^{-2}	2.461×10^{-3}	2.30×10^{-2}	$L = 10$	1.04×10^{-2}	8.305×10^{-3}	3.40×10^{-1}
	(1.08×10^{-2})		(2.44×10^{-2})		(0.79×10^{-2})		(2.86×10^{-1})
$L = 30$	1.34×10^{-3}	2.684×10^{-4}	8.00×10^{-3}	$L = 30$	1.62×10^{-3}	1.298×10^{-3}	1.33×10^{-1}
	(1.14×10^{-3})		(8.26×10^{-3})		(1.01×10^{-3})		(1.18×10^{-1})
$L = 50$	4.70×10^{-4}	9.397×10^{-5}	4.87×10^{-3}	$L = 50$	5.95×10^{-4}	4.760×10^{-4}	7.86×10^{-2}
	(4.06×10^{-4})		(4.98×10^{-3})		(3.37×10^{-4})		(7.41×10^{-2})
$L = 100$	1.13×10^{-4}	2.256×10^{-5}	2.46×10^{-3}	$L = 100$	1.14×10^{-4}	1.143×10^{-4}	3.88×10^{-2}
	(1.01×10^{-4})		(2.49×10^{-3})		(0.97×10^{-4})		(3.85×10^{-2})
$L = 300$	1.20×10^{-5}	2.402×10^{-6}	8.31×10^{-4}	$L = 300$	1.42×10^{-5}	1.138×10^{-5}	1.31×10^{-2}
	(1.11×10^{-5})		(8.33×10^{-4})		(1.10×10^{-5})		(1.32×10^{-2})
$L = 500$	4.21×10^{-6}	8.412×10^{-7}	4.93×10^{-4}	$L = 500$	4.90×10^{-6}	3.921×10^{-6}	7.94×10^{-3}
	(4.01×10^{-6})		(5.00×10^{-4})		(3.92×10^{-6})		(7.94×10^{-3})

as $j = L + 1 (j = 0)$. Results for the associated distribution, $p(x)$, are shown in Fig. 5(b) for $\langle X_0\rangle = 0.8$ and $L = 50$. There is a higher probability for half-integer positions than for integer positions which is understood since in the regime of nearly completely filled pore, only half-integer positions can be adopted. A more detailed analysis follows noting that a separation s between the rightmost B and leftmost R occurs with probability $\langle X_0\rangle(1 - \langle X_0\rangle)^s$. From this one concludes that the ratio of probabilities for half-integer versus integer positions is given by $1/(1 - \langle X_0\rangle) = 5$. This fine structure is washed out in a coarse-grained picture again producing a uniform distribution except near pore openings.

Additional analysis for $\langle X_0\rangle = 0.8$ and $L = 100$ shows similar edge effects where the deviation from a uniform distribution is apparent within ten cells of the pore ends.

D. Generalized tracer diffusivity for SFD

For SFD with $\langle X_0\rangle = 0.8$, results for $D_{\rm tr}(j, j+1)$ versus j are shown in Fig. 6 for $L = 10, 30, 100$, and 300. We highlight the enhanced values near the left end of the pore by just showing behavior in this end region rather than the entire pore. However, the development of a plateau with smaller $D_{\rm tr}$ value in the pore center is also clear for all these cases. The insets show evolution of $\mathrm{Var}(N_B)$ and $\mathrm{Cov}(B_{L/2}, B_{L/2+1})$ from the random initial state. As indicated in the introduction to Sec. IV, these latter results are used to estimate the onset of the steady-state regime (denoted by a vertical dotted line). Only after this onset are data analyzed to determine steady-state values for J_B and $\nabla\langle B_j\rangle$ which are used to evaluate $D_{\rm tr}(j, j+1)$. For contrast with the above analysis, we also present results in Fig. 7 for SFD with a lower $\langle X_0\rangle = 0.2$ where the effects of the SFD constraint are less severe. Correspondingly, $D_{\rm tr}(j, j+1)$ values are significantly higher. Note also that the steady state is achieved significantly more quickly (by a factor of $\sim$10) for $\langle X_0\rangle = 0.2$ relative to $\langle X_0\rangle = 0.8$.

In Table I, we provide additional information pertaining to these simulations. Precise KMC values for $\langle R_1\rangle$ are compared with estimates $\langle R_1\rangle \approx [(L-1)^2 + (L-1)\langle X_0\rangle]^{-1}$, modifying (12) using Ref. [16] for $D_{\rm tr}$(min) and $\nabla\langle R_{j\gg L/2}\rangle \approx \langle X_0\rangle/(L-1)$ (cf. [31]). KMC values do reveal the weak dependence on $\langle X_0\rangle$ suggested in our previous discussion. Also presented are precise KMC values for the flux J_B, obtained from directly counting the number of B's desorbing from the

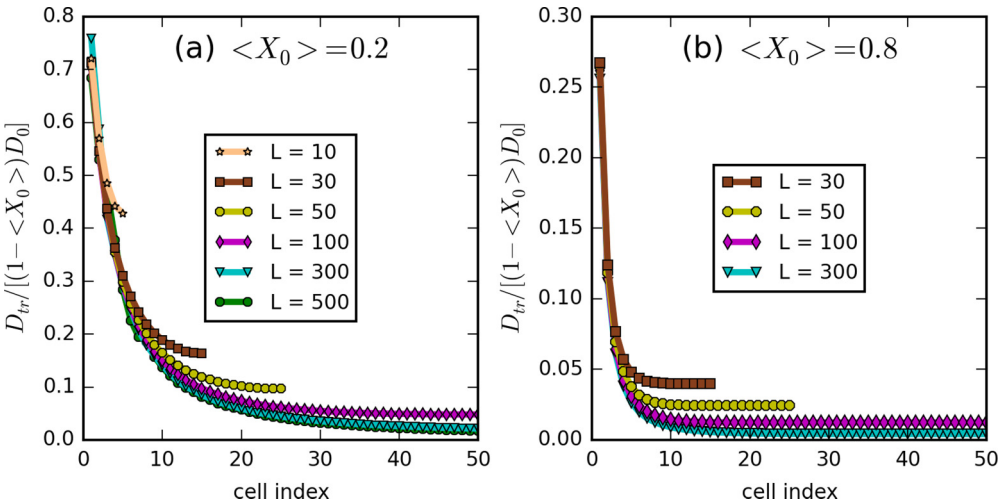

FIG. 8. Comparison of the rescaled $D_{\rm tr}(j, j+1)$ for SFD for the left half of the pore for various pore lengths shown. (a) $\langle X_0\rangle = 0.2$; (b) $\langle X_0\rangle = 0.8$.

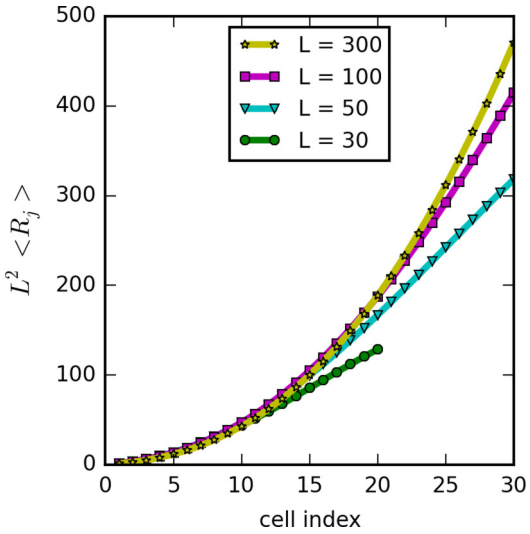

FIG. 9. Scaling of concentration profile near the pore opening for SFD with $\langle X_0\rangle = 0.2$: $L^2\langle R_j\rangle$ versus cell index j for various L.

right end of the pore. We find essentially identical values for the J_B are obtained from $J_B = w_{\rm des}\langle B_L\rangle = w_{\rm des}\langle R_1\rangle$. Finally, we give precise KMC values for $D_{\rm tr}$(min) and compare them with reliable estimates from the slightly modified version of (1) given in Ref. [16].

Next, we provide a more detailed discussion and assessment of the *enhanced generalized tracer diffusivity* near the pore end, as well as of the convergence of these enhanced values to well-defined limiting behavior for a semi-infinite pore as $L\to\infty$. To understand the enhancement, we argue that fluctuations associated with adsorption-desorption processes (which couple the pore interior to the well-stirred exterior reservoirs) naturally induce $D_{\rm tr}$ values closer to mean-field predictions near the pore openings. Furthermore, it is reasonable to expect that the site-approximation estimate, $D_{\rm tr}(\text{site}) = D_0(1-\langle X_0\rangle)$, for SFD from (5) provides an upper bound on all $D_{\rm tr}(j,j+1)$, and in particular on $D_{\rm tr}(\max) = \max D_{\rm tr}(j,j+1) = D_{\rm tr}(1,2)$. The factor $1-\langle X_0\rangle$ simply reflects blocking of hopping by empty sites, but this formulation neglects any "back-correlation" in diffusion which generally produces lower values of $D_{\rm tr}$ [32]. In fact, for large L, we find that

$$D_{\rm tr}(\max)/D_{\rm tr}(\text{site}) = 0.742\,(0.273) \;\text{ for }\; \langle X_0\rangle = 0.2\,(0.8). \tag{24}$$

Thus, as might be expected, mean-field type behavior is more closely achieved for lower $\langle X_0\rangle$ where SFD effects are reduced. Since for $D_{\rm tr}(\max) = D_{\rm tr}(1,2)$ both cells are inside the pore, one might further argue that behavior should be even better captured by a mean-field type pair approximation which to some extent accounts for correlations between NN pairs of sites. The corresponding estimate of tracer diffusivity is $D_{\rm tr}(\text{pair}) = (2-\langle X_0\rangle)(2+\langle X_0\rangle)^{-1}D_{\rm tr}(\text{site})$ [19]. Thus, for large L, we find that

$$D_{\rm tr}(\max)/D_{\rm tr}(\text{pair}) = 0.907\,(0.650) \;\text{ for }\; \langle X_0\rangle = 0.2\,(0.8), \tag{25}$$

so indeed this pair approximation captures the maximum effective tracer diffusivity significantly better than the site approximation.

We now consider limiting behavior for large L. Figure 8 compares on the same plot $D_{\rm tr}(j,j+1)$ values for different pore lengths. For $\langle X_0\rangle = 0.2$ where $D_{\rm tr}(j,j+1)$ decays more slowly into the pore, the convergence to a limiting form as $L\to\infty$ is particularly clear. For $\langle X_0\rangle = 0.8$, the more rapid decay tends to hide this feature, but it does still apply. As indicated in Sec. III C, this behavior is associated with a scaling of the concentration profile near the pore end of the form $\langle R_j\rangle \approx r(j)/L^2$ for large L, with $r(1) = O(1)$ and where $r(j)$ is independent of L. This latter behavior is shown in Fig. 9 for $\langle X_0\rangle = 0.2$. It is apparent that the function $r(j)$ exhibits a faster than linear polynomial-type increase with j. From (13), one obtains

$$\begin{aligned} D_{\rm tr}(j,j+1) &= -J_R/\nabla\langle R_j\rangle \\ &\approx h(1-\langle X_0\rangle)r(1)/[r(j)-r(j-1)] \\ &\approx h(1-\langle X_0\rangle)r(1)/[dr(j)/dj], \end{aligned} \tag{26}$$

thus indicating algebraic decay with increasing j.

Finally, we compare results from the above TCP analysis with that in Refs. [19,20] based on a suitably defined time to exit the pore, $T_j(\langle X_0\rangle)$, for a tagged walker (TW) starting at site j. Specifically, one defines a generalized tracer diffusion coefficient for each site j as $D_{\rm tr}(j) = T_j(0)/T_j(\langle X_0\rangle)$. However, there is some arbitrariness (in contrast to the TCP approach) in the definition of exit time, and thus in the TW determination of $D_{\rm tr}(j)$. Furthermore, one cannot directly compare with the "more natural" results for TCP where $D_{\rm tr}(j,j+1) = D_{\rm tr}(j,j+1)|_{\rm TCP}$ is defined for NN pairs of sites (rather than for single sites). However, it is reasonable to assign the TW estimate of $D_{\rm tr}(j,j+1)$ as $D_{\rm tr}(j,j+1)|_{\rm TW} =$

TABLE II. Comparison of TCP and TW predictions for generalized tracer diffusivity, $D_{\rm tr}(j,j+1)$, for SFD with $L = 100$ and $\langle X_0\rangle = 0.8$ and 0.2. One also finds that $D_{\rm tr}(\min) = 0.00246$ (0.00287) for TCP (TW) when $\langle X_0\rangle = 0.8$, and $D_{\rm tr}(\min) = 0.039$ (0.066) for TCP (TW) when $\langle X_0\rangle = 0.2$.

$\langle X_0\rangle =$ 0.8	$D_{\rm tr}(j,j+1)/D_0$ *TCP*	$D_{\rm tr}(j)/D_0$ *TW*	$D_{\rm tr}(j,j+1)/D_0$ *TW*	$\langle X_0\rangle =$ 0.2	$D_{\rm tr}(j,j+1)/D_0$ *TCP*	$D_{\rm tr}(j)/D_0$ *TW*	$D_{\rm tr}(j,j+1)/D_0$ *TW*
$j=1$	0.0524	0.0928	0.0653	$j=1$	0.562	0.810	0.757
$j=2$	0.0229	0.0378	0.0293	$j=2$	0.431	0.705	0.645
$j=3$	0.0129	0.0208	0.0171	$j=3$	0.342	0.584	0.530
$j=4$	0.0084	0.0134	0.0114	$j=4$	0.281	0.476	0.430
$j=5$	0.0061	0.0094	0.0082	$j=5$	0.233	0.385	0.349
$j=6$	0.0048	0.0070	0.0063	$j=10$	0.120	0.168	0.159

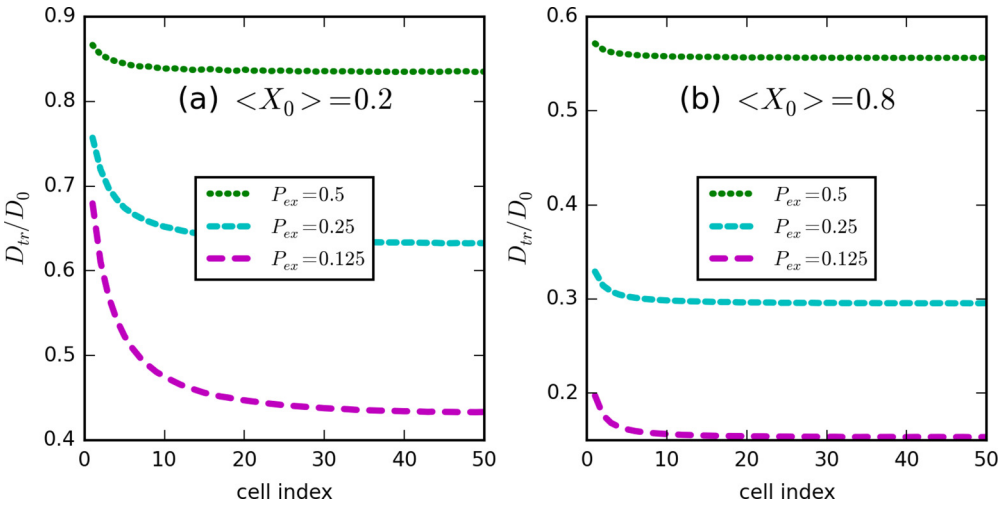

FIG. 10. Generalized tracer diffusion coefficient $D_{\rm tr}(j,j+1)/D_0$ versus j for the left half of a pore with $L=100$ for selected values of $P_{\rm ex}>0$ (shown): (a) $\langle X_0\rangle=0.2$; (b) $\langle X_0\rangle=0.8$.

$\frac{1}{2}[D_{\rm tr}(j)+D_{\rm tr}(j+1)]$. Also, the TW approach has some advantages in applying directly to semi-infinite systems, and also in elucidating the form of $D_{\rm tr}(j)\sim D_{\rm tr}(j,j+1)|_{\rm TW}\sim 1/j^2$ decay at least for large $\langle X_0\rangle$ with strong SFD effects. In Table II, we compare predictions from the TW and TCP approaches for $D_{\rm tr}(j,j+1)$ near the pore opening for $L=100$. While there is some minor difference in numerical values from the two approaches, they are consistent in describing the key trends in behavior.

E. Behavior with passing $P_{\rm ex}>0$

Finally, we comment briefly on behavior for $P_{\rm ex}>0$ which corresponds to relaxing the SFD constraint. Note that now one no longer has a simple characterization of configurations in the steady-state ensemble with B particles to the left and R to the right separated by a localized interface. We have performed detailed analysis for $P_{\rm ex}=0.25$. The key observation is that even introducing "smaller" nonzero value of $P_{\rm ex}$ dramatically reduces the development of spatial correlations relative to SFD. Thus, we find that $\mathrm{Var}(N_B)=\mathrm{Var}(N_R)$ remains close to the initial value given by (5), where again $\mathrm{Var}(N_X)=L\langle X_0\rangle(1-\langle X_0\rangle)$ is exactly time invariant.

Next, we present results for the generalized tracer diffusivity $D_{\rm tr}(j,j+1)$ in Fig. 10 for various $P_{\rm ex}>0$. Again, one finds a plateau in the pore center with enhanced values near the pore end. Now, the plateau value $D_{\rm tr}(\min)$ depends only weakly on pore length, L, and remains finite in the limit $L\to\infty$. As noted in Sec. III C, behavior of $D_{\rm tr}(\min)$ which corresponds to the nonzero tracer diffusion coefficient for an infinite pore is characterized in Ref. [30]. From Fig. 10, one finds that there is only weak enhancement of $D_{\rm tr}(j,j+1)$ for larger $P_{\rm ex}$, but enhancement becomes stronger approaching the SFD regime for smaller $P_{\rm ex}$. In all cases, the maximum enhanced value $D_{\rm tr}(\max)=D_{\rm tr}(1,2)$ is bounded above by the mean-field estimate $D_{\rm tr}(\text{site})=D_0[(1-\langle X_0\rangle)+P_{\rm ex}\langle X_0\rangle]$ from (5). However, the latter is quite close to $D_{\rm tr}(\max)$ for larger $P_{\rm ex}$ and lower $\langle X_0\rangle$.

V. CONCLUSIONS

We have provided a comprehensive analysis of TCP for a stochastic model of diffusive transport through a narrow linear pore of finite length where differently colored red (R) and blue (B) particles adsorb at opposite ends of the pore and desorb from either end. We consider passing of species within the pore to be inhibited, and focus on the case where passing is excluded (single-file diffusion). The following features are characterized: (i) quasilinear concentration profiles of R and B particles and associated diffusion fluxes through the pore; (ii) particle number fluctuations within the pore; (iii) associated NN pair correlations of R and B particles within the pore; (iv) location of the interface between regions in the pore populated by R and B particles; and, significantly, (v) determination of the generalized tracer diffusivity and detailed analysis of its behavior including enhancement near pore openings and associated scaling of concentration profiles in that region.

The generalized tracer diffusivity provides a comprehensive characterization of transport within the pore, and has been shown to be invaluable in elucidating behavior of more complex reaction-diffusion processes [19,20,25,30]. From the broader perspective on nonequilibrium systems and steady states, it is instructive to provide a complete characterization of these states. As indicated above, we have performed such an analysis for TCP, specifically characterizing particle number fluctuations and spatial correlations.

ACKNOWLEDGMENTS

This work was supported by the U.S. Department of Energy (USDOE), Office of Basic Energy Sciences, Division of Chemical Sciences, Geosciences, and Biosciences through the Ames Laboratory Chemical Physics program. The work was performed at Ames Laboratory which is operated for the USDOE by Iowa State University under Contract No. DE-AC02-07CH11358.

APPENDIX A: KMC SIMULATION ALGORITHM

We utilize a rejection-free simulation algorithm where at each simulation step, some process is implemented and the probability that a specific process is implemented is proportional to the physical rate of that process. Time is advanced by an incremental amount, $\Delta t = -\ln(x_{\rm ran})/R_{\rm tot}$, where $R_{\rm tot}$ denotes the total rate of all processes at that stage in the simulation, and $x_{\rm ran}$ is a random number uniformly distributed on (0,1]. Just tracking behavior once the system has reached a steady state, we use an ergodic average to calculate probabilities of various configurations. For example, one has

$$\langle C_j \rangle = \sum_{1 \leqslant m \leqslant N} C_j \Delta t_m / \sum_{1 \leqslant m \leqslant N} \Delta t_m, \tag{A1}$$

where simulation steps are labeled by m (and N is the total number of steps), and again $C_j = 1(0)$ if cell j is occupied by a particle of type C (otherwise). In the simplest approach, one could check the state of each cell after each simulation step and update the sums appropriately. However, in each simulation step the state of no more than two cells changes, so this approach is quite inefficient.

Instead, to develop a more efficient algorithm focused on updating only when cells change state, we track the time at which each cell's state was last changed. Specifically, we create a listing of the last modified time for each cell. At the end of the equilibration phase we set the values for all cells to the current time, which is the start of the production part of the simulation. These times are updated every time a cell's state changes. At any time, the time a particle has been in the cell is the current time less our stored time of when the cell's status last changed. At each simulation step, this value is calculated only for the cells where a change occurs. Those values are added to the accumulated statistics. At the end of the simulation, the occupancy time is calculated for all cells and added to the accumulated total. Failure to do so would omit the current configuration from the averaging.

This method ensures that the time spent on calculating statistics for each simulation step is independent of the size of the system, compared to the simple method which requires more time for larger systems. The cost of this faster method is the additional bookkeeping. For all but the smallest system sizes, this overhead should be significantly less than the time saved by not updating occupancy times for cells that have not changed state.

APPENDIX B: GENERALIZED TCP FORMULATIONS

In a more general formulation of TCP, the reservoir at the left end of the pore has a concentration $f\langle X_0\rangle$ of B particles and $(1-f)\langle X_0\rangle$ of R particles. The reservoir at the right end has a concentration $f\langle X_0\rangle$ of R particles and $(1-f)\langle X_0\rangle$ of B particles. Since the reservoirs are infinite, these concentrations do not change either during initial transient behavior or in the steady state. We naturally restrict our attention to $\frac{1}{2} < f < 1$. Detailed specification of the model follows that presented for the standard formulation analyzed in this paper which corresponds to $f = 1$. The main difference from $f = 1$ for the general case $\frac{1}{2} < f < 1$ is that now both B and R particles can adsorb into both ends of the pore. Specifically, the rate of B [R] adsorption to empty cells at the left end of the pore is given by $w_{\rm adsL}(B) = hf\langle X_0\rangle$[$w_{\rm adsL}(R) = h(1-f)\langle X_0\rangle$]. R [B] adsorption to empty cells at the right end of the pore is given by $w_{\rm adsR}(R) = hf\langle X_0\rangle$[$w_{\rm adsR}(B) = h(1-f)\langle X_0\rangle$]. Desorption rates for either species at either end of the pore remain as $w_{\rm des} = h(1-\langle X_0\rangle)$.

The more general formulation does not provide independent information from the standard formulation for $f = 1$. The linearity of the master equations describing behavior of the stochastic model, together with the linearity of the boundary conditions specifying adsorption-desorption kinetics, implies a simple relationship between behavior for $\frac{1}{2} < f < 1$ and $f = 1$. See also below. For example, it is natural to define excess concentrations, $\langle \delta C_j\rangle$, and naturally rescaled versions, $\langle C_j^*\rangle$, of these as

$$\langle \delta C_j\rangle = \langle C_j\rangle - (1-f)\langle X_0\rangle \text{ and}$$
$$\langle C_j^*\rangle = (2f-1)^{-1}\langle \delta C_j\rangle \text{ for } C = B \text{ and } R. \tag{B1}$$

Then, the above-mentioned linearity implies that $\langle C_j^*\rangle = \langle C_j\rangle|_{f=1}$.

For general $\frac{1}{2} < f < 1$, generalized tracer diffusivity is still determined from (13); i.e., $D_{\rm tr}(j,j+1) = -J_B/\nabla\langle B_j\rangle = -J_R/\nabla\langle R_j\rangle$. For example, J_B can be determined from the difference between desorption and adsorption rates at the right end of the pore:

$$J_B = w_{\rm des}\langle B_L\rangle - w_{\rm adsR}(B)(1-\langle X_0\rangle) = w_{\rm des}(2f-1)\langle B_L^*\rangle. \tag{B2}$$

It also follows from (B1) that $\nabla\langle B_j\rangle = (2f-1)\nabla\langle B_j^*\rangle$. Thus, it immediately follows that $D_{\rm tr}(j,j+1)$ is independent of f. We have checked this result comparing simulation values obtained for $f = 1$, $f = 0.8$, and $f = 0.6$.

Finally, the simple relationship between behavior for $\frac{1}{2} < f < 1$ and $f = 1$ deriving from the linearity of the master equations and boundary conditions extends to multicell probabilities. In fact, this is a feature needed for rigorous proof of the above claims.

APPENDIX C: TCP ANALYSIS FOR OTHER MODELS OF DIFFUSIVE DYNAMICS

The TCP formulation for assessing tracer diffusivity in a porous system of finite width is quite general, applying for many possible prescriptions of diffusive dynamics. One simple modification to the current model would be to introduce a different hop rate, $h' \neq h$, for adsorption and desorption at the pore ends, where the rate h still describes hopping to NN empty cells within the pore. With this choice, the equilibrium state of the system still has a common uniform total density of particles inside and outside the pores. The case $h' \ll h$ is of some physical relevance reflecting possible slow desorption from the porous material [18].

A significantly different prescription of diffusive dynamics implemented by Nelson and Auerbach [18] uses a two-dimensional lattice to describe the porous material allowing the possibility of anisotropic diffusion within the material. Specifically, one can introduce distinct rates h_x for hopping in the x direction across the porous material, and h_y for

hopping in the orthogonal direction. (In simulations, one would impose periodic boundary conditions for the porous material of finite size in the y direction.) Introducing an anisotropic diffusion ratio, $\eta = h_y/h_x$, it is clear that $\eta = 0$ reduced to a one-dimensional SFD model analogous to that treated in this paper. Even for $\eta \ll 1$, SFD is relaxed as differently labeled particles can pass each other in two dimensions. Diffusion in this case is mediated by vacancies. An interesting feature of this model noted in Ref. [18] is that for $\eta \gg 1$ with rapid diffusion in the y direction relative to the x direction, any correlation between hopping in the x direction is washed out by facile hopping in the y direction. Thus, one finds mean-field behavior in this regime where $D_{\rm tr}(j, j+1) = D_0(1 - \langle X_0 \rangle)$.

[1] A. L. Hodgkin and R. D. Keynes, J. Physiol. (London) **128**, 61 (1955).

[2] E. J. Harris, *Transport and Accumulation in Biological Systems* (Academic Press, London, 1960).

[3] E. J. A. Lea, J. Theor. Biol. **5**, 102 (1963).

[4] L. Reikert, in *Advances in Catalysis*, edited by D. D. Eley, H. Pines, and P. B. Weisz (Academic Press, New York, 1970), Vol. 21, p. 281.

[5] J. Kärger, M. Petzold, H. Pfeiffer, S. Ernst, and J. Weitkamp, J. Catal. **136**, 283 (1992).

[6] T. E. Harris, J. Appl. Probab. **2**, 323 (1965).

[7] V. Gupta, S. S. Nivarthi, A. V. McCormick, and H. T. Davis, Chem. Phys. Lett. **247**, 596 (1995).

[8] K. Hahn, J. Kärger, and V. Kukla, Phys. Rev. Lett. **76**, 2762 (1996).

[9] V. Kukla, J. Kornatowski, D. Demuth, I. Girnus, H. Pfeifer, L. V. C. Rees, S. Schunk, K. K. Unger, and J. Kärger, Science **272**, 702 (1996).

[10] T. Meersmann, J. W. Logan, R. Simonutti, S. Caldarelli, A. Comotti, P. Sozzani, L. G. Kaiser, and A. Pines, J. Phys. Chem. A **104**, 11665 (2000).

[11] M. Dvoyashkin, H. Bhase, N. Mirnazari, S. Vasenkov, and C. R. Bowers, Anal. Chem. **86**, 2200 (2014).

[12] L. Heinke, D. Tzoulaki, C. Chmelik, F. Hibbe, J. M. van Baten, H. Lim, J. Li, R. Krishna, and J. Kärger, Phys. Rev. Lett. **102**, 065901 (2009).

[13] D. G. Levitt and G. Subramanian, Biochim. Biophys. Acta **373**, 132 (1974).

[14] H. van Beijeren, K. W. Kehr, and R. Kutner, Phys. Rev. B **28**, 5711 (1983).

[15] H. Hahn and J. Kärger, J. Phys. Chem. B **102**, 5766 (1998).

[16] D.-J. Liu, J. Wang, D. Ackerman, I. I. Slowing, M. Pruski, H.-T. Chen, V. S.-Y. Lin, and J. W. Evans, ACS Catal. **1**, 751 (2011) suggested the refinement $D_{\rm tr} \approx D_0(1 - C)/[1 + C(L - 1)]$ for smaller CL.

[17] P. H. Nelson and S. M. Auerbach, J. Chem. Phys. **110**, 9235 (1999).

[18] P. H. Nelson and S. M. Auerbach, Chem. Eng. J. **74**, 43 (1999).

[19] D.-J. Liu, A. Garcia, J. Wang, D. M. Ackerman, C.-J. Wang, and J. W. Evans, Chem. Rev. **115**, 5979 (2015).

[20] D. M. Ackerman, J. Wang, and J. W. Evans, Phys. Rev. Lett. **108**, 228301 (2012).

[21] S. Vasenkov and J. Kärger, Phys. Rev. E **66**, 052601 (2002).

[22] H. Spohn, J. Phys. A **16**, 4275 (1983).

[23] J. W. Evans, Phys. Rev. B **41**, 2158 (1990).

[24] J. E. Santos and G. M. Schutz, Phys. Rev. E **64**, 036107 (2001).

[25] A. Garcia, J. Wang, T. L. Windus, A. D. Sadow, and J. W. Evans, Phys. Rev. E **93**, 052137 (2016).

[26] One might randomly populate the pore with any shape of concentration profile decreasing from left to right (right to left) from $\langle X_0 \rangle$ to 0 for B (R), so that the total population is fixed at $\langle X_0 \rangle$. One such simple special case is to randomly populate the left half of the pore with B and the right half with R, both at concentration $\langle X_0 \rangle$. In this case, (7) is replaced by $\mathrm{Var}(N_B) = \mathrm{Var}(N_R) = \frac{1}{2} L \langle X_0 \rangle [1 - \langle X_0 \rangle]$ at $t = 0$.

[27] R. Kutner, Phys. Lett. A **81**, 239 (1981)

[28] H. Spohn, *Large Scale Dynamics of Interacting Particles* (Springer, Berlin, 1991).

[29] J. Quastel, Commun. Pure Appl. Math. **45**, 623 (1992).

[30] J. Wang, D. M. Ackerman, V. S.-Y. Lin, M. Pruski, and J. W. Evans, J. Chem. Phys. **138**, 134705 (2013); see Fig. 2.

[31] Modified estimates for the concentration gradient, $\nabla \langle R_{j \approx L/2} \rangle \approx \langle X_0 \rangle/(L+1), (\langle X_0 \rangle - \langle R_1 \rangle)/L$, and $(\langle X_0 \rangle - 2\langle R_1 \rangle)/(L-1)$, come from considering pairs of cells $j = 0$ and $L + 1, j = 0$ and L (or $j = 1$ and $L + 1$), and $j = 1$ and L, respectively. Here $j = 0 (j = L + 1)$ denotes the cells just outside the left (right) end of the pore.

[32] H. van Beijeren and K.W. Kehr, J. Phys. C: Solid State Phys. **19**, 131 (1986).